'87 KACC 1987.10.16～17

TRAJECTORY CONTROL OF ROBOT MANIPULATORS USING VSS THEORY
----- SMOOTHING MODIFICATION -----

Hideki Hashimoto, Kwee-bo Sim, Jianxin Xu, and F.Harashima

Institute of Industrial Science, University of Tokyo
7-22-1, Roppongi, Minato-ku, Tokyo 106, JAPAN

ABSTRACT

A new control algorithm using the VSS theory is developed for accurate trajectory control of robot manipulators. This paper focuses on the implementation of VSS controller with smoothing laws in the design of effective tracking control for robotic arms. The VSS controller for multi-linkage robot arm is realized using balance condition and its simplification which possesses powerful smoothing capability to reduce or even remove undesireble chattering and meanwhile keep the robust characteristic to reject system uncertainties. The design principle of selecting different smoothing methods, which aims at achieving trade-off between smoothng and robust behaviors while considering the actual system constraints, is also given and further confirmed through experimental results.

1.INTRODUCTION

It is well known that VSS has strong robustness of feedback stability in the presence of system uncertainties such as parametric variations or disturbance [1] [2] . The main drawback of this kind of control is that the resulting control input is discontinuous on the predetermined switching surface and consequently the control input chatters at a theoretically infinite frequency. To overcome this problem, much effort has been devoted to exploit smoothing methods to reduce or remove the chattering while the whole control system remains robust. A feasible method is to replace the discontinuous switching law by a proper continuous one [3] .

Balance condition is one of these deliberately developed proposals, which is derived from the careful consideration on the bandwidth of plant dynamics and VSS controller [4] [5] . The boundary of interpolating control input is changed according to the balance condition and the system becomes to perform the desired behavior.

There is, however, one significant problem in practice that confines its application to complex control situations, that is, the balance condition is time-consuming due to its complex calculation if comparing with other smoothing algorithms [3] [7] . Such a control law, besides being difficult to realize in practice , might even not be directry applicable to the multi-linkage arm. It is thus necessary to simplify the control law, and find the applicable situations so as to achieve a trade-off between tracking precision and available computing speed. In other words, it is natural to use simple smoothing methods to obtain both tracking precision and robustness with high sampling frequency. On the other hand, a simplified balance condition will be an excellent candidate if sampling frequency is constrained to below some value in practice, and such a sampling interval is as long as possible for real-time computation of the control algorithm. This is because that the balance condition method possesses powerful smoothing capability, hence it still has efficient effect as to reduce chattering with low sampling frequency whereat other smoothing methods will either fail to reduce the chattering or lose the robustness, thereafter lose the tracking accuracy. This gives the design principle in order to achieve the trade-off between the smoothing behavior and tracking precision. Taking a two-linkage robotic arm as exsample, the remain of this paper will show how to select control strategies, whatever simplified balance condition or others, and provide several simulation as well as experimental results for analysis and comparison.

2.SMOOTHING IMPLEMENTATION WITH BALANCE CONDITION

In this section a brief discription about smoothing implementation of conventional VSS controller is given in which the improvment is achieved by introducing balance condition [5] .

Consider the following differential equation

$$x^{(n)}(t)=f(X;t)+b(X;t)u(t)+d(t) \tag{1}$$

where $u(t)$ is the control input, x is the scalar output, and $X=(x,\dot{x},\cdots,x^{(n-1)})^t$ is the state vector. We assume that the sliding mode control based on VSS is well-known here, and therefore we omit the explanation of VSS and sliding mode. Chattering is in general highly undesirable in practice, since it involves extremely high control activity, and further may excite high-frequency dynamics neglected in the course of modeling. We can remedy this situation by smoothing out the control discontinuity in a thin boundary layer neighboring the switching surface:

$$B(t)=\{X,\ |s(X,t)|\leqq\Phi\}\ ;\Phi>0 \tag{2}$$

where Φ is the boundary layer thickness, and $\varepsilon:=\Phi/\lambda^{n-1}$ is the boundary layer width (Fig.1). Control smoothing is achieved by choosing outside of $B(t)$ control law u so as to guarantee boundary layer attractiveness, i.e. trajectories starting inside $B(t=0)$ remain inside $B(t)$ for all $t\geqq 0$. A continuous control law to approximate switched control is achieved by interpolating u inside $B(t)$, as illustrated in Fig.2., to replace the general used sign function $sgn(s)$. As proved in [5] , this operation leads to tracking to within a guaranteed precision ε, and more generally guarantees that for all trajectories starting inside $B(t=0)$

$$|x^{(i)}(t)|\leqq(2\lambda)^i\varepsilon \qquad i=0,\ldots,n-1 \tag{3}$$

Further, as shown in [5] , smoothing control discontinuity inside $B(t)$ essentially assigns a lowpass filter structure to local dynamics of the variable s, thus eliminating chattering. Recognizing this filter structure allows us to tune up the control law so as to achieve a trade-off between tracking precision and robustness to unmodeled dynamics. Boundary layer thickness Φ is made to be time-varying, and is monitored so as to always exploit the maximum control bandwidth available. In order to maintain attractiveness of the boundary layer, now that Φ is allowed to vary with time we must actually modify attraction condition (4) into (5).

$$\frac{1}{2}\frac{d}{dt}s^2(x;t)\leqq-\eta|s| \tag{4}$$

$$|s|\geqq\Phi \quad\Rightarrow\quad \frac{1}{2}\frac{d}{dt}s^2\leqq(\dot{\Phi}-\eta)|s| \tag{5}$$

This modification is derived easily as follows:

We separate the region $|s|\geqq\Phi$ into two regions such as

$$s^+=s-\Phi(>0)\ ,\ s^-=s+\Phi(<0) \tag{6}$$

In each region, the attraction condition (4) is expressed as

$$\begin{array}{lll} s^+>0\rightarrow\dot{s}^+\leqq-\eta & \rightarrow\dot{s}-\dot{\Phi}\leqq-\eta & \rightarrow\dot{s}\leqq\dot{\Phi}-\eta \\ s^-<0\rightarrow\dot{s}^-\geqq-\eta & \rightarrow\dot{s}-\dot{\Phi}\geqq-\eta & \rightarrow\dot{s}\geqq\dot{\Phi}-\eta \end{array} \tag{7}$$

From (7), we get the modified condition (5).

The addition term $\dot{\Phi}|s|$ in (5) reflects the fact that the boundary layer attraction condition is more

stringent during boundary layer contraction $\dot{\Phi}<0$ and less stringent during boundary layer expansion $\dot{\Phi}>0$. In order to satisfy (5), the quantity $-\Phi dot$ is added to control discontinuity gain $k(X;t)$, i.e. in our smoothed implementation, the term $k(X;t)sgn(s)$ obtained from switched control law u is actually replaced by $\bar{k}(X;t)sat(s/\Phi)$, where:

$$\bar{k}(X):=k(X)-\dot{\Phi} \tag{8}$$

Accordingly, control law u becomes:

$$u=\hat{u}-\bar{k}(X)sat(s/\Phi) \tag{9}$$

where $\hat{u}$ is the estimated compensation that represents feedforward control. Consider now the system trajectories inside the boundary layer, where they lie by construction: they can be expressed directly in terms of the variable s as

$$\dot{s}=-\bar{k}(X)s/\Phi+\{-\Delta f(X)+d(t)\} \tag{10}$$

where $\Delta f:=\hat{f}-f$, and $\hat{f}$ is the predicted value of f. Now since $\bar{k}$ and Δf are continuous in X, we can exploit (3) to rewrite (10) in the form:

$$\dot{s}=-\bar{k}(X_d)s/\Phi+\{-\Delta f(X_d)+d(t)+O(\varepsilon)\} \tag{11}$$

We see from (11) that the variable s (which is a measure of the algebraic distance to the surface $S(t)$) is the output of a stable first-order filter, whose dynamics only depends on the desired state $X_d(t)$ and perhaps explicitly on time, and whose inputs are (to first order) 'perturbations', namely disturbance $d(t)$ and uncertainty $\Delta f(X_d;t)$. Chattering is thus indeed eliminated, as long as high-frequency unmodeled dynamics are not excited. The dynamics structure of the closed-loop system is summarized in Fig.3: perturbations are filtered according to (11) to give s, which in turn provides tracking error $\tilde{x}(:=x-x_d)$ by further lowpass filtering, according to definition (3). Control u is a function of X and X_d. Now, since λ is the break-frequency of filter $s(X;t):=(d/dt+\lambda)^{n-1}\tilde{x}$ it must be chosen to be '*small*' with respect to high-frequency unmodeled dynamics (such as unmodeled structural modes or neglected time delays). Further, we can now tune boundary layer thickness Φ so that (11) also represents a first-order filter of bandwidth λ. It suffices to let $\bar{k}(X_d;t)/\Phi:=\lambda$ which can be written from (8) as

$$\dot{\Phi}+\lambda\Phi=k(X_d;t) \tag{12}$$

Equation (12) defines the desired time-history of boundary layer thickness Φ, and in the light of figure 3 shall be referred to as the balance condition. Intuitively it amounts to tune up the closed-loop system so that it mimics an n-th order critically damped system. Further, definition (8) can then be rewritten as:

$$\bar{k}(X;t):=k(X;t)-k(X_d;t)+\lambda\Phi \tag{13}$$

3. DESIGN STRATEGIES OF ROBOTIC ARMS

Most of the robotic arms are serial linkage manipulators with high nonlinearity on and complicated interactions between each joints [8] . Therefore in the design of effective position or trajectory controller for robotic arms, it is of importance to take into account the robustness against system uncertainties, which in fact guarantees the tracking accuracy implicitly. Moreover, a robust controller will make it possible only to consider simplified dynamics of robotic arms, concequentaly avoid using sophisticated on-line computational schemes. Based on such a consideration, in this section we will give the design procedures of VSS controller with balance condition in turn for one-linkage and two-linkage arms, then simplify the two-linkage case by ignoring the interactive inferences except for some important parametric variations, e.g. the payload term, and the gravity term which is easy to be computed. The validity will be investigated in following section.

3-1. Control implimentation of one-linkage arm [6]

Consider a simple one-linkage arm

$$\ddot{\theta}=b\{-(\xi+b_0/r^2)\dot{\theta}-(ml+ML)g\sin\theta\}+bu \tag{14}$$

$$b=(I+ML^2+J/r^2)^{-\frac{1}{2}}$$

θ - angle
$\dot{\theta}$ - angular velocity
m - link weight
M - payload weight
l - the center of link gravity
L - the length of link
I - link inertia
J - equivalent inertia of gear and servo motor shaft
r - gear ratio
ξ - viscous coefficient of gear
b_0 - viscous coefficient of servo motor
u - control input

The range of variable payload is set as $0\leqq M\leqq M_0$,

and the uncertainty of viscous damping force is assumed as

$$(1-\delta)(\hat{\xi}+\frac{\hat{b}_0}{r^2})\leqq\xi+\frac{b_0}{r^2}\leqq(1+\delta)(\hat{\xi}+\frac{\hat{b}_0}{r^2}),0\leqq\delta\leqq1. \tag{15}$$

We select the switching surface s=0 so that the position response shows integral control while keeping sliding mode. Such switching surface is as

$$s=\dot{\tilde{\theta}}+2\lambda\tilde{\theta}+\lambda^2\int_0^t\tilde{\theta}d\tau,\tilde{\theta}=\theta-\theta_d \tag{16}$$

The control input u is composed of nonlinear compensation term and saturating function term as follows

$$u=\hat{b}^{-1}[\hat{u}-\bar{k}sat(s/\Phi)] \tag{17}$$

The nonlinear compensation term is of the form

$$\hat{u}=\hat{b}[(\hat{\xi}+\frac{\hat{b}_0}{r^2})\dot{\theta}+(ml+\hat{M}L)g\sin\theta]+\ddot{\theta}_d-2\lambda\dot{\tilde{\theta}}-\lambda^2\tilde{\theta} \tag{18}$$

$$\hat{b}=\{(I+M_0L^2+J/r^2)\cdot(I+J/r^2)\}^{-\frac{1}{2}} \tag{19}$$

The saturating function term is composed of a saturating function and control gain

$$\bar{k}=k(\theta)-k(\theta_d)+\lambda\Phi/\beta \tag{20}$$

$$k(\theta)=\hat{b}[(1+\delta)|(\hat{\xi}+\hat{b}_0/r^2)\dot{\theta}|+\hat{M}Lg|\sin\theta|]+\beta\eta$$
$$+(\beta-1)|\ddot{\theta}_d-2\lambda\dot{\tilde{\theta}}-\lambda^2\tilde{\theta}| \tag{21}$$

$$\beta=[\frac{I+M_0L^2+J/r^2}{I+J/r^2}]^{\frac{1}{2}} \tag{22}$$

The boundary layer thickness Φ varies in accordance with the following law:

$$k(\theta_d)\geqq\frac{\lambda k}{\beta}\quad=>\quad\dot{\Phi}+\lambda k=\beta k(\theta_d)$$

$$k(\theta_d)\leqq\frac{\lambda k}{\beta}\quad=>\quad\dot{\Phi}+\frac{\lambda\Phi}{\beta^2}=\frac{k(\theta_d)}{\beta} \tag{23}$$

3-2. Control implementation of two-linkage arm

Consider the two-linkage arm of Fig.4. The physical model of the robotic arm has the form

$$M(\theta)\ddot{\theta}+h(\theta,\dot{\theta})=\tau \tag{24}$$

where $M(\theta)\in R^{2\times 2}$ is the inertia matrix, $h(\theta,\dot{\theta})\in R^2$ represents nonlinear terms such as Coriolis', centrifugal forces, gravity and viscous damping forces. As related previously, the available model is in fact to be the form

$$\hat{M}(\theta)\ddot{\theta}+\hat{h}(\theta,\dot{\theta})=\tau \tag{25}$$

where the symbol ' $\hat{}$ ' denotes the estimation. The discrepancies between (24) and (25) may arise from well known factors : imprecisions on the robot arm geometry or inertias, uncertainties on friction terms or the loads, etc. The sliding controller for robot arm (24) then takes the form

$$\tau=\hat{M}(\theta)u+\hat{h}(\theta,\dot{\theta}) \tag{26}$$

where the components u_i $(i=1,2)$ are defined as

$$u_i=G_i(\theta)\{\hat{u}_i-\bar{k}_i(\theta,\dot{\theta})sat(s_i/\Phi_i)\} \tag{27}$$

In equation (26) and (27), the design guideline is similar to that of the forgoing one-linkage case except for the gain $k_i(\theta,\dot{\theta})$, which must take into account the additional interaction terms from coupling inertias existed in matrix $M(\theta)$ and vector $h(\theta,\dot{\theta})$.

As described by [5] in detail, a sufficient solution of gain vector $k=[k_1,k_2]$ can be obtained from following relation

$$A(\theta,\dot{\theta})k(\theta,\dot{\theta})=k^*(\theta,\dot{\theta}) \tag{28}$$

The matrix $A(\theta,\dot{\theta})$ is defined as

$$\begin{bmatrix} 1 & -\beta_1 G_2\Delta_{12}\,|\,sat(\frac{s_2}{\Phi_2})\,| \\ -\beta_2 G_2\Delta_{21}\,|\,sat(\frac{s_1}{\Phi_1})\,| & 1 \end{bmatrix} \tag{29}$$

Further, each component of $k^*(\theta,\dot{\theta})$ is defined to be

$$k_i^*(\theta,\dot{\theta})\geq\beta_i\{\,|\,\hat{u}_i\,|\,(1-\beta_i^{-1})+\beta_i+\sum_{j\neq i}G_j\Delta_{ij}\,|\,\hat{u}_j-\{\frac{\lambda\Phi_j}{\beta_j}$$

$$-k_j(\theta_d,\dot{\theta}_d)\}\,sat(\frac{s_j}{\Phi_j})\,|+\eta_i\} \tag{30}$$

where the scalars δ_i and Δ_{ij} are defined such that, for all θ

$$\delta_i\geq\sum_{j=1}^{2}|\,\bar{m}_{ij}(\theta)\,|\cdot|\,h_j(\theta)-\hat{h}_j(\theta)\,| \tag{31}$$

$$\Delta_{ij}\geq|\sum_{l=1}^{2}\bar{m}_{il}(\theta)\cdot\hat{m}_{lj}(\theta)\,| \tag{32}$$

and $\bar{m}_{ij}(\theta)$ is the component of $M^{-1}(\theta)$ located at the ith row and jth colum.

3-3. Simplification of the two-linkage design

As seen in section 3-2, even for a two-linkage robotic arm the complicated computation is needed to generate the torques required to support a desired motion in the case of using balance condition. From the design procedure it is obvious that in this computational algorithm both the inverse dynamics and modeling error should be taken into consideration, which in the multi-linkage case is especially time costing due to the calculation of coupling control gains and predicted control inputs. On the contrary, it should be noted that the inertia matrix of robotic arm is diagonal elements of generally dominate other coupling terms, thus the coupling control component can be accounted for by the controller robustness.

Notice that gain $k_i(\theta,\dot{\theta})$ must actually verify

$$k_i(\theta,\dot{\theta})\geq\beta_i(\,|\,\hat{u}_i\,|\,(1-\beta_i)^{-1}+\delta_i+\sum_{j\neq i}\Delta_{ij}\,|\,u_j\,|+\eta_i) \tag{33}$$

Compare equation (33) with equation (22), we find that the latter can be derived from the former first by neglecting the coupling term Δ_{ij} $(i\neq j)$, which is essencially the combination of non-diagonal elements of inertia matrix, as can be seen from equation (32), second by neglecting all the centrifugal and coriolis' forces and then computing the gravity of each link independently. These simplifications will obviously cause unpleasant influence to robot control system. Fortunately this problem is somewhat mitigated in the case of geared robotic arm, since the effects of time-varying inertia are reduced by a factor r_i^2, where r_i is the gear ratio, while the interaction torques and nonlinear torques such as centrifugal and coriolis are similarly scaled down by r_i when reflected to the servo motors. Finally it should point out that the guaranteed robustness properties of VSS controller allow one to design simple controller without losing perfect tracking capability.

According to these reasons, we simplify the control algorithm of two-linkage robotic arm by partially decoupling the control system, that is, both controllers for upper and lower link are designed individually in terms of the one-linkage arm as mentioned at section 3-1, except for the gravity terms.

4. ANALYSIS OF SIMULATION AND EXPERIMENT RESULTS

We now describe the application of the above development to the robust feedback control of a two-linkage robotic arm. For comparison and analysis another smoothing control strategy implemented by using continuous function [4] is also executed on the same robotic arm to obtain required experimental results.

4-1. Control system of two-linkage arm

Description of experiment system

The control system is shown in Fig.5. Each dc servo motor is fed by a PWM power MOSFET chopper amplifier operating at 10KHz. A 1000pulse/rev. shaft encoder is used to sense the output psition, while a dc tachogenerator coupled directly to the servo motor provides an analogue signal for the output speed.

Desired path

In order to examine the validity of proposed methods, the whole system is forced to move along the desired path (Fig.6), namely, a straight line in two-dimentional work space. The desired velocity pattern of the end-point of the arm is given in Fig.7.

The corresponding trajectories of upper and lower links in joint space are illustrated in Fig.8.

Smoothig control laws

Two different smoothing control laws are used in this paper.

One is to replace the discontinuous switching logic by a proper contiuous function as follows [3]

$$sgn(s_i)\rightarrow conti(s_i)=\frac{s_i}{|\,s_i\,|+\delta_i},\ \delta_i>0\quad i=1,2 \tag{34}$$

This replacement is shown in Fig. 9 when δ_i is equal to zero, $conti(s_i)$ becomes $sgn(s_i)$ and when δ_i is large, $conti(s_i)$ is going to zero.

Another is the before discussed balance condition in which the switching logic is replaced by a saturating function (Fig.10)

$$sgn(s_i)\rightarrow sat(s_i)=\begin{cases}\frac{s_i}{\Phi_i} & if\ |\,s_i\,|\leq 1\\ sgn(s_i) & otherwise\end{cases} \tag{35}$$

where Φ_i is a variable scalar that reflects the

time-history of control requirment with respect to the given trajectories.

Determination of design parameters

The slope of switching surface λ_i, boundary layer thicness Φ_i (which is dependent on the value η_i of attraction condition (5)) and constant δ_i are the most important parameters in the design of VSS controller using smoothig strategies (34) and (35).

The slope of switching surface λ is selected according to the following constraints:

$$\lambda \leqq \lambda_R \fallingdotseq \frac{2\pi}{3}\nu_R \ , \ \lambda \leqq \lambda_A \fallingdotseq \frac{1}{3T_A} \ , \ \lambda \leqq \lambda_S \fallingdotseq \frac{1}{5}\nu_{sampling} \qquad (36)$$

where ν_R is the frequency of the lowest unmodeled structural resonant mode, T_A is the largest unmodeled time-delay in the actuator and $\nu_{sampling}$ is the sampling rate.

In our system, λ_A is about 400, λ_S is 40 (since the lowest sampling rate is set up at 200Hz) and λ_R is assumed to be larger than λ_S. Therefore λ is selected to be lower than its superior limit λ_S. On the other hand, the larger the λ, the faster the system responds and the better the tracking accuracy will be. Based on above consideration as well as the available input limitation, λ is finally selected to be 40 in our simulation.

As for η_i, this value determines the time of convergence to the surface $s_i=0$; the time to converge becomes to be shorter as η_i is set up at larger and larger value. Furthermore, from equation (22) and (23) it is easy to observe that the boundary layer thickness Φ_i will be approximately proportional to the rate η_i/λ_i provided the break-frequency λ_i is sufficient high in contrast to the frequency of desired trajectory. In order to mitigate the saturation influence caused from selecting large λ_i , large η_i is selected as remedy since the boundary layer width is widened. In this paper, η_i is selected at least as large as λ_i to achieve the trade-off.

The constants δ_i (i=1,2) are set to be 0.1 - 0.5 to achieve the compromise between robustness and smoothness.

4-2. Simulation of two-linkage arm

Before going to the comparison of foregoing related smoothing control laws, we first examine whether or not the simplification of balance condition is still valid for parametric uncertainties, nonlinear interaction or unknown payload, etc. Under the condition that all the sensors have infinitesimal resolution and no delay, simulations of two-linkage arm are carried out to compare the system responses with or without using the simplified control algorithm, although this condition is impossible in actual system, in simulation no problem will take place to effect the validity of comparison results.

Case 1 is the non-simplified control strategy which is described in section 3-2.

Case 2 is the simplified control strategy which is described in section 3-3.

The simulation results for the two cases are shown in Table 1, which accounts for the maximum tracking error with respect to the two cases while changing the sampling frequency and payload. Sampling time are chosen 1msec, 3msec and 5msec respectively, for simplicity both the slope of switching surface λ_i and design parameter η_i are set up to be 40 according to the parameter design principle. The arm and actuater inertias are assumed within 20 percent uncertainties around their physical values. The payload assumes varying from 0kg to 3kg with the predicted value being 1.5kg

According to the Table 1, we notice that in both cases the tracking error is very small with respect to the desired path, this means that, in spite of the significant simplification on the control algorithm the whole system keeps sufficient robustness and accurate tracking ability while the sampling period and payload change their values.

Fig.11 and Fig.12 illustrate the tracking error $e_i(t)$, sliding surfaces $s_i(t)$, boundary layer thckness $\Phi_i(t)$ and control input torques $u_i(t)$ with respect to case 1 and case 2 separately. From both cases we can observe that the boundary layers $\Phi_i(t)$-trajectories and sliding surface $s_i(t)$-trajectories represent a time varying measure of the validity of the assumptions on model uncertainties with time. In those figures we also know that $s_i(t)$-trajectories are varying within boundary layers $\Phi_i(t)$. It means that both control activities directly depends on $s_i(t)/\Phi_i(t)$.

As the conclusion of simulation results, we confirm that the simplified VSS controller with balance condition is valid on the aspects of guaranteeing the accurate tracking response and robust performance, hence in next section the experimental comparison constrains to between the algorithm with simplified balance condition and that with continuous function

4-3. Experiment of two-linkage arm

In experiment the main obstacle is the contradiction among the real-time computation and the complexity of control algorithm. Therefore in this section all the experiments, the comparison between the two smoothing methods, are arranged according to different sampling rates.

For both the control schemes, Table 2 gives the control design parameters. Similar to the simulation case, 20 percent uncertainty of inertias and ± 1.5kg variations of payload around the predicted 1.5kg are assumed in control design procedures. The experiment of two-linkage arm are carried out for three cases as follows:

Case 1 : Sampling time is 1.25 msec
Case 2 : Sampling time is 2.5 msec
Case 3 : Sampling time is 5 msec

Table 3 gives the comparison of maximum tracking errors between the two smoothing methods. In case 1, however, even the simplified balance condition can not be computed on-line due to its complexity, hence the maximum tracking error of the upper and lower arms are represented only with the continuous function.

Fig.13 and 14 illustrate the tracing responses for both the schemes concerning case 2 and case 3 separately. From Fig.13 we can observe the chattering phenomenon when using continuous function. On the contrary almost no chattering yields by using the balance condition.

Fig.14 shows that the continuous function does not suit the case because violent chattering generated. By deliberately choosing the design parameter δ_i , e.g., selecting (δ_1=1,δ_2=0.8), the chattering can be reduced to the same degree as the case with simplified balance condition, nevertheless the tracking error is about twice as large as that of balance condition. On the other hand, one can see that the simplified balance condition is still valid even though there exists some chattering in control input.

Comparing the smoothing law using balance condition with the one using continuous function, it is obvious that how to select a proper control law is depending on whether the candidate is potential to be implemented to actual system, that is, it should be simple enough for real-time computation with available sampling frequency. Hence the design principle is, it is reasonable to take priority of selecting continuous function, simplified balance condition and balance condition in turn as far as higher sampling frequency is available. All the conclusion can be drawn from experimental results.

5.CONCLUSION

In this paper the algorithm of practical robust VSS control using balance condition and its simplification are presented. The validity of

simplified modification is confirmed through simulation and experiment results of a two degree of freedom robotic arm.

Comparison results shows the correct design principle of selecting different smoothing methods as to modify VSS controllers: the appropriate choice of control algorithm is depending on considering trade-off between system control requirements and hardware limitations, in this paper the determination is made to keep the "balance" among the smoothness of control inputs, robustness of system behaviors, accuracy of tracking responses and simplisity of computational schemes.

REFERENCE

[1] V.I.Utkin, "Variable Structure System, Present and Future," Auto. and Remote Control, 3.5, 1983.

[2] H.Hashimoto, F.Harashima, "Variable Structure Strategy In Motion Control-Industrial Applications," IFAC, Vol.3, pp.57-62, July, 1987

[3] F.Harashima, H.Hashimoto, K.Maruyama, "Practical Robust Control of Robot Arm Using Variable Structure System," Proceedings of Robotics and Automation Conference, pp.532-539, April, 1986.

[4] J.J.E.Slotine, "The Robust Control of Robot Manipulators," Int. J. Robotics Research, pp.49-64, 1985.

[5] H.Asada, J.J.E.Slotine, Robot Analysis and Control , John Wiley and Sons, 1986.

[6] H.Hashimoto, J.X.Xu, F.Harashima "Practical Design of VSS Controller Using Balance Condition," Proceedings of Robotics and Automation Conference, pp.2039-2046, March, 1987.

[7] H.Hashimoto, K.Maruyama, F.Harashima "A Microprocessor-Based Robot Manipulator Control with Sliding Mode," IEEE Trans. on Industrial Electronics,Vol.ie-34, No.1, pp.11-18, Feb.1987.

[8] R.P.Paul "Robot Manipulators: Mathematics, programing and control," MIT Press, 1981.

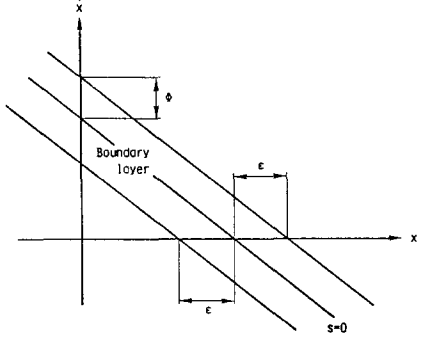

Fig. 1. Construction of the boundary layer

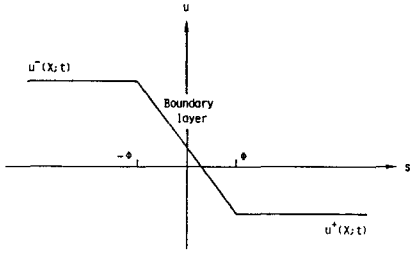

Fig. 2. Interpolation of the control law in the boundary layer

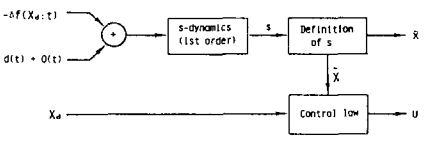

Fig. 3. Dynamic structure of the closed loop system

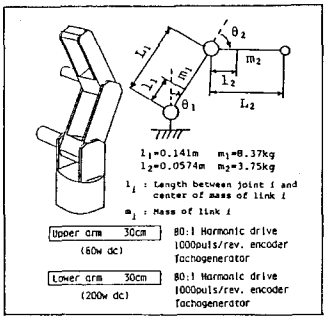

Fig. 4. Two-linkage robotic arm

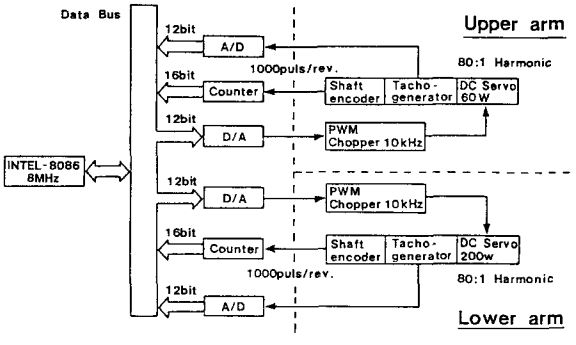

Fig. 5. Control system of the two-linkage arm

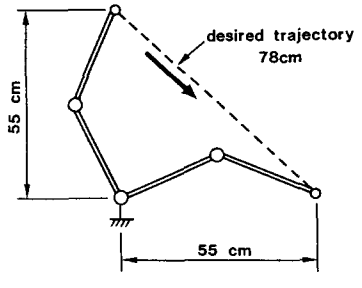

Fig. 6. Desired path of the End-point of the two-linkage arm

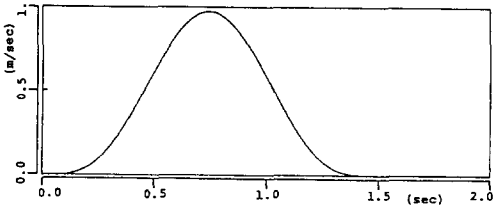

Fig. 7. Velocity pattern of the desired path

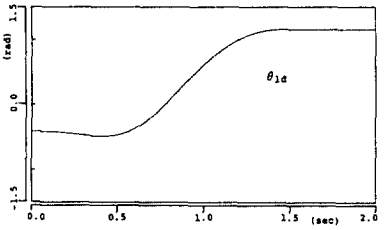

(a) Trajectory of lower link

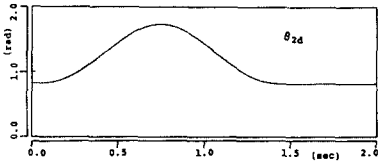

(b) Trajectory of upper link

Fig. 8. The angular position of desired trajectories in joint space

Table 2. Control design parameters

Parameter / Link	η	λ	δ
Upper	80	20	0.1
Lower	480	20	0.4

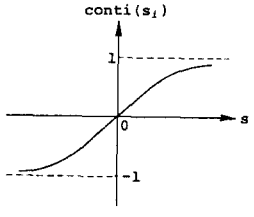

Fig. 9. Continuous function of s

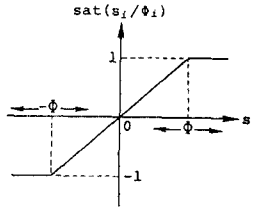

Fig. 10. Saturating function of s with variable boundary layer

Table 1. Simulation result (Comparison of maximum tracking error)

(unit : x 10^{-4}[rad])

Link	a \ c / b	Non-simplified Control 1	3	5	Simplified Control 1	3	5
Upper Link	0	-0.653	1.062	1.160	1.493	1.742	1.882
	1.5	0.839	1.404	1.552	1.262	1.258	1.393
	3	1.043	1.765	1.973	1.076	1.366	1.922
Lower Link	0	0.772	0.755	0.684	0.769	1.775	2.239
	1.5	0.712	0.681	0.594	0.769	1.775	2.239
	3	0.633	0.679	1.001	0.769	1.775	2.239

* a : Payload[kg] , b : Sampling Time[msec] , c : Control Strategy

Table 3. Experiment result (Comparison of maximum tracking error)

(unit : x 10^{-2}[rad])

Link	a \ c / b	Continuous function 1.25	2.5	5	Balance condition 1.25	2.5	5
Upper link	0	-3.14	-2.97	-3.63	-	-1.75	1.92
	1.5	-2.27	-1.75	3.32	-	-1.66	2.09
	3	2.27	2.44	3.32	-	2.09	3.32
Lower link	0	-0.401	-1.01	-1.62	-	1.75	1.47
	1.5	-0.297	-0.593	-1.64	-	1.75	1.52
	3	-0.262	-0.363	-1.75	-	1.75	1.61

* a : Payload[kg] , b : Sampling time[msec] , c : Control strategy

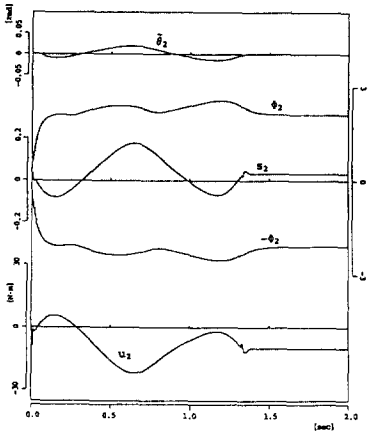

(Fig. 11-a) Tracking performance of upper link

Fig. 11. Tracking error, boundary layer hypersurface and control input of two-linkage link (Non-simplified balance condition) Payload : 3 kg , Sampling time : 5 msec

Fig. 12. Tracking error, boundary layer, hypersurface and control input of tow-linkage link (Simplified balance condition) Payload : 3 kg , Sampling time : 5 msec

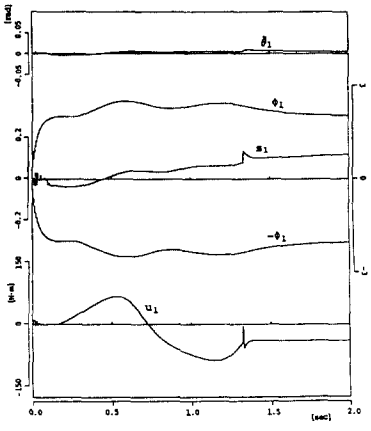

(Fig. 11-b) Tracking performance of lower link

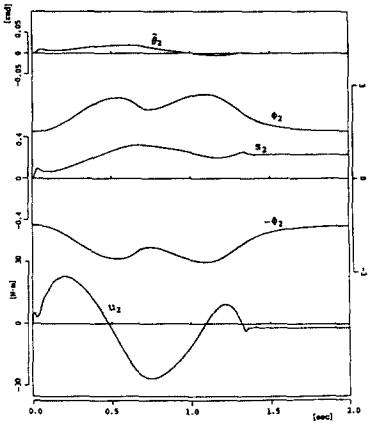

(Fig. 12-a) Tracking performance of upper link

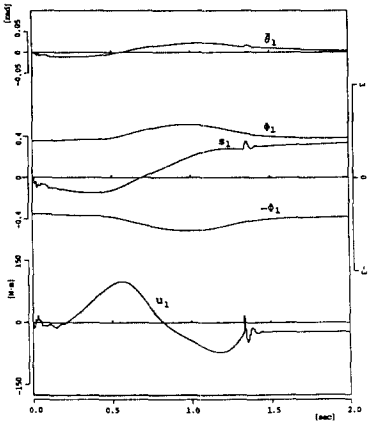

(Fig. 12-b) Tracking performance of lower link

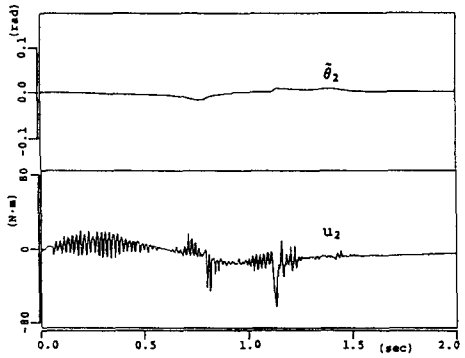

(a) Tracking error and control torque of upper link (Continuous function)

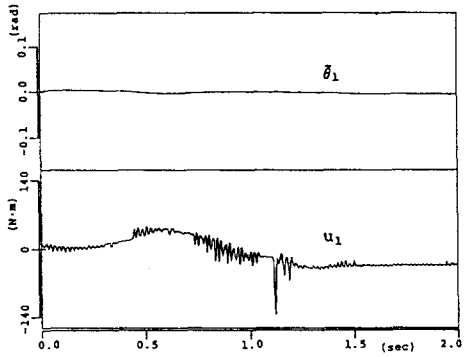

(b) Tracking error and control torque of lower link (Continuous function)

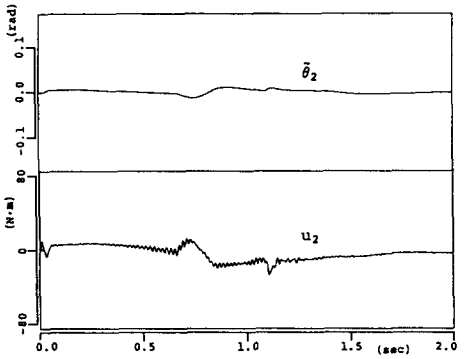

(c) Tracking error and control torque of upper link (Simplified balance condition)

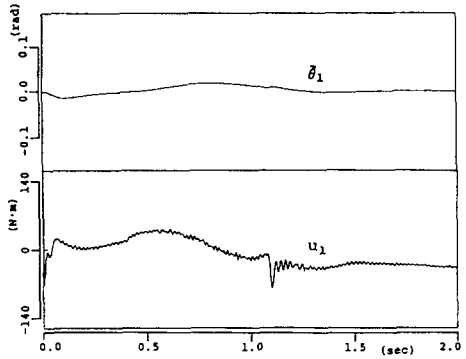

(d) Tracking error and control torque of lower link (Simplified balance condition)

Fig. 13. Experiment result in case 2
(Payload : 1.5 kg , Sampling time : 2.5 msec)

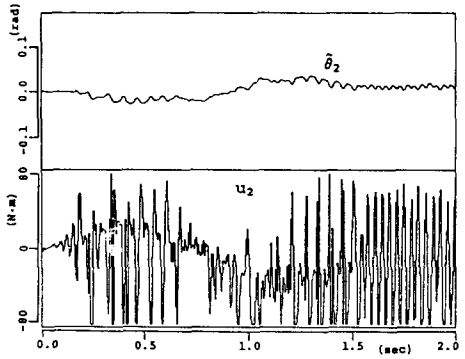

(a) Tracking error and control torque of upper link (Continuous function)

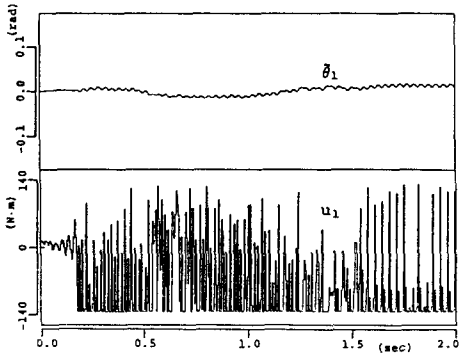

(b) Tracking error and control torque of lower link (Continuous function)

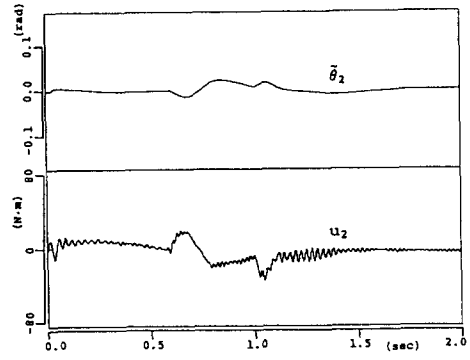

(c) Tracking error and control torque of upper link (Simplified balance condition)

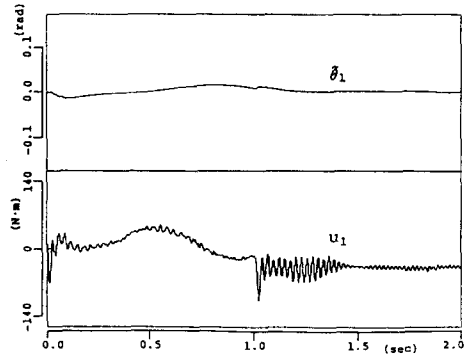

(d) Tracking error and control torque of lower link (Simplified balance condition)

Fig. 14. Experiment result in case 3